Magnetocaloric properties and Griffiths phase of ferrimagnetic cobaltite $CaBaCo_4O_7$

Tina Raoufi[1,2], Jincheng He(何金城)[1,2], Binbin Wang(王彬彬)[1,2], Enke Liu(刘恩克)[1,2], and Young Sun(孙阳)[1,3,†]

[1] *Beijing National Laboratory for Condensed Matter Physics, and Institute of Physics, Chinese Academy of Sciences, Beijing* 100190, *China*
[2] *School of Physical Sciences, University of Chinese Academy of Sciences, Beijing* 100190, *China*
[3] *Center of Quantum Materials and Devices, Chongqing University, Chongqing* 401331, *China*

(Received 25 July 2022; revised manuscript received 29 August 2022; accepted manuscript online 5 September 2022)

We present a study on the magnetocaloric properties of a $CaBaCo_4O_7$ polycrystalline cobaltite along with research on the nature of magnetic phase transition. The magnetization as a function of temperature identifies the ferrimagnetic to paramagnetic transition at a Curie temperature of 60 K. Moreover, a Griffiths-like phase is confirmed in a temperature range above T_C. The compound undergoes a crossover from the first to second-order ferrimagnetic transformation, as evidenced by the Arrott plots, scaling of the universal entropy curve, and field-dependent magnetic entropy change. The maximum of entropy change is 3 J/kg·K for $\Delta H = 7$ T at T_C, and a broadening of the entropy peak with increasing magnetic field indicates a field-induced transition above T_C. The analysis of the magnetic entropy change using the Landau theory reveals the second-order phase transition and indicates that the magnetocaloric properties of $CaBaCo_4O_7$ are dominated by the magnetoelastic coupling and electron interaction. The corresponding values of refrigerant capacity and relative cooling power are estimated to be 33 J/kg and 42 J/kg, respectively.

Keywords: magnetocaloric effect, cobaltite, phase transition, Griffiths phase

PACS: 75.40.Cx, 75.50.–y **DOI:** 10.1088/1674-1056/ac8f39

1. Introduction

Global warming has made society more aware of the need to reduce its energy consumption. Since living standards and economic growth are improved along with the increasing population, the demand for cooling technology and thermal energy harvesting systems is expected to increase substantially over the next 30 years. Refrigeration accounts for a substantial portion of global electricity consumption. Therefore, improving energy conversion efficiency is crucial in this branch of technology. The magnetic refrigeration and cryogenic systems based on the magnetocaloric effect (MCE) are a viable alternative to traditional gas-compression refrigeration because of their high thermodynamic performance, low noise, and environmental friendliness.[1,2] Magnetic refrigeration technology around room temperature is important for household refrigeration and air conditioner, but magnetic refrigeration in low-temperature regions is essential for liquefaction of helium, hydrogen, and nitrogen, which is commonly used in low-temperature physics, superconductors, medicine, and space technology.[3,4]

The MCE is a magneto-thermodynamic character for magnetic solid materials, which represents the reversible temperature variation or entropy change when it is magnetized or demagnetized under adiabatic or isothermal conditions.[5] The MCE is regarded as an inherent effect in magnetic materials when a magnetic material is exposed to magnetic fields. Up to date, the magnetic properties and magnetocaloric efficiency of a wide range of magnetic materials with various characterization and preparation techniques such as oxides, alloys, amorphous, intermetallic, and composites have been investigated and reviewed in literature.[6–8]

In recent years, the oxide $CaBaCo_4O_7$ (CBCO), which belongs to the "114" cobaltite from a new class of geometrically frustrated magnets, has attracted interest due to its complex geometrically frustrated network. The CBCO compound crystallizes in the orthorhombic $Pbn2_1$ symmetry in the entire temperature range from the room temperature to 4 K.[9] The magnetic unit cell of CBCO includes four equivalent Co sites, leading to an alternate stacking of two types of corner shared CoO_4 tetrahedral: Co1 sits in the triangular layer, while Co2, Co3, and Co4 atoms are in the kagome layer, causing considerable magnetic frustration.[10,11] The geometrical frustration in the kagome and triangular lattice of this compound can be partially lifted due to large orthorhombic structural distortion and charge ordering (the stoichiometric formula $CaBaCo_2^{+2}Co_2^{+3}O_7$), leading to a ferrimagnetic order state below 60 K.[12]

In this work, the magnetic and magnetocaloric properties of the 114 cobaltite $CaBaCo_4O_7$ compound are studied with the aims at better understanding the low-temperature physical properties of CBCO and developing new magnetic materials for magnetic refrigeration. We use comprehensive magneti-

[†]Corresponding author. E-mail: youngsun@cqu.edu.cn

© 2023 Chinese Physical Society and IOP Publishing Ltd

zation calculation to describe the magnetic phase transition by applying the Banerjee criterion, as well as recent methods such as universal scaling and a quantitative technique based on the field dependence of the magnetic entropy change to find the order of magnetic phase transition to gain a better understanding of the nature of magnetic transitions and MCE properties of the system.

2. Experiments

Polycrystalline samples of $CaBaCo_4O_7$ were synthesized by the conventional solid-state reaction method. The stoichiometric quantities of all the initial reactants with high-purity, including $CaCO_3$, $BaCO_3$, and Co_3O_4, were ground in an agate mortar for 2 h, and then heated at 900 °C in air for 12 h for decarbonization. After another 1 h grinding process, the mixture was then pressed in the form of cylindrical bars to make pellets, heated in air at 1100 °C for 14 h, and finally cooled down to room temperature.

The temperature-dependent dc magnetization and magnetization versus applied magnetic field up to 7 T were measured by using a Quantum Design magnetic properties measurement system (MPMS). The crucial MCE characteristics, such as $-\Delta S_M(T)$, refrigerant capacity (RC), and relative cooling power (RCP), were calculated from the magnetization versus applied magnetic fields.

3. Results and discussions

3.1. Structural characterization

The structural properties of the CBCO samples were investigated by using the x-ray diffraction (XRD) at room temperature. Figure 1 shows the diffraction pattern of a CBCO sample and Rietveld refinement analysis using the FullProf program.

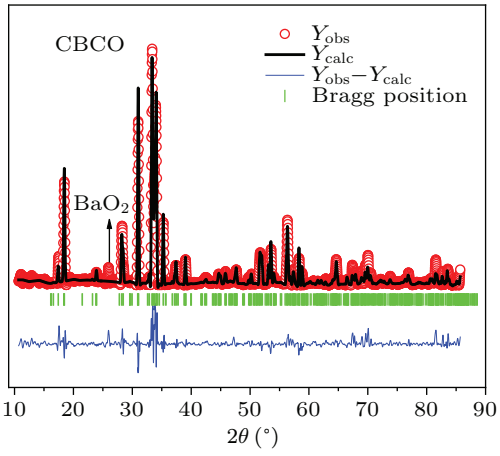


Fig. 1. The x-ray diffraction pattern of the prepared $CaBaCo_4O_7$ sample at room temperature.

The results of the refinement demonstrate that the sample crystalizes in the orthorhombic crystal structure with the $Pbn2_1$ space group and the cell parameters $a = 6.277(1)$ Å, $b = 10.987(9)$ Å, $c = 10.180(9)$ Å, and $V = 702.198(5)$ Å^3. In comparison to previous work, the value of the volume was decreased.[13] There is also a small extra peak related to BaO_2 in the XRD pattern. The sintering temperature and annealing time are important factors in the solid-state reaction process. The grain size grows as the annealing time and sintering temperature increase. The variation in annealing time in the process of preparing our sample compared to the work of Dhansekhar *et al.* could explain the decrease in volume cell and observation of inhomogeneity (extra peak) in XRD.[14–16]

3.2. Magnetic characterization

Figure 2(a) displays the FC magnetization for polycrystalline CBCO measured as a function of temperature in 0.05 T magnetic field over a temperature range of 20–300 K. The FC curve exhibits a sharp increase of magnetization at the Curie temperature (T_C) of a ferrimagnetic (FIM) to paramagnetic (PM) transition.[17] The temperature derivative of the M–T curve is shown in the inset of Fig. 2(a), which can be used to unambiguously calculate T_C. The value of T_C is evaluated to be 60 K, which is close to other reports.[16,17] One of the principal capabilities of the CBCO compound is that the structural distortion lifts exchange-interaction frustration which leads to the unique geometry of the kagome lattice. The exchange interaction in the system would be influenced by the precise $Co^{3+}/Co^{2+} = 1$ ratio, resulting in the appearance of the FIM ordering.[10,12]

The inverse magnetic susceptibility versus temperature is presented in Fig. 2(b). The linear behavior of χ^{-1} versus T at higher temperatures suggests that χ^{-1} obeys the Curie–Weiss (CW) law in this region:[18]

$$\chi^{-1} = \frac{T - \theta_P}{C}, \tag{1}$$

where θ_P is the CW temperature, and C is the Curie constant. The black line in Fig. 2(b) depicts the fit to the CW law with parameters $\theta_P = 13.6$ K and $C = 1.1010$ K·A·m^2/T·kg. The small value of the CW temperature is expected for the ferrimagnetic state.[19] The small value of intercept can be referred to competition between AFM and FM phase interaction before the Griffiths temperatures (T_G) and the persistence of inhomogeneity in the PM regime. The assumption that χ^{-1} does not follow the CW law above T_C is evident from this diagram. The downturn behavior of inverse susceptibility versus temperature above T_C is clear from Fig. 2(b), which is considered as a sign of Griffiths phase (GP) singularity rather than a pure PM region. The appearance of short-range FM/AFM correlation well above T_C is signaled by the faster reduction of χ^{-1} below T_G.

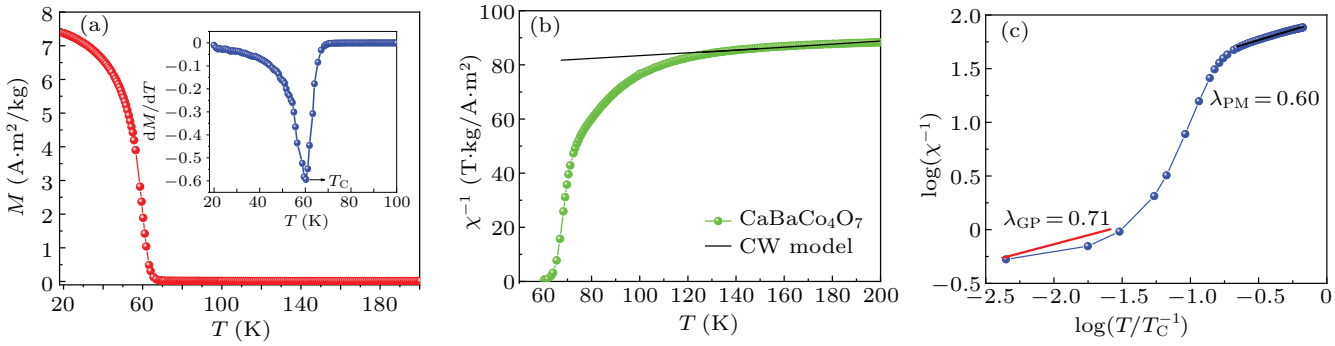


Fig. 2. (a) Magnetization as a function of temperature in the field-cooled mode under a magnetic field of 0.05 T. The inset presents the dM/dT versus T curves. (b) Temperature evolution of inverse magnetic susceptibility. The black solid line indicates the linear fit to the CW law. (c) The T-dependent susceptibility data following Eq. (2), plotted in double logarithmic scale.

The exponent λ, which can be calculated from the following equation, is commonly used to evaluate the Griffiths phase:[20]

$$\chi^{-1} \propto (T - T_C^R)^{1-\lambda}, \tag{2}$$

where λ is a constant to obtain the degree of deviation from the CW behavior and T_C^R is the critical transition temperature of the random ferromagnetic where susceptibility diverges. The choice of $T_C^R = \theta_P$ is generally good one because it ensures $\lambda \sim 0$ in the paramagnetic region. The difference between T_C and θ_P in the present system makes it reasonable to choose $T_C^R = T_C$. In Fig. 2(c) the log–log plot shows the power-law behavior in $\chi^{-1}(T)$ and the slope of the fitted straight line [Eq. (2)] gives the λ_{GP} and λ_{PM} values. The value of λ_{PM} is estimated to be zero in the pure PM regime. Here, λ_{PM} is positive and less than unite, and $T_C < T_C^R < T_G$, which confirm the appearance of GP. Susceptibility measurements were carried out in another magnetic field to establish the feature and to identify the magnetic field limit where the Griffith phase disappeared. Griffith phase is present even in the high magnetic field of 7 T (the results are not shown here).

Previous research demonstrated that the strong AFM Co–Co interaction facilitated by Co–O–Co super-exchange in kagome and triangular layers generates complex magnetic properties in CBCO. Because of the critical function of significant structural distortion, cobalt valence, and charge ordering in forming a long-range magnetic order, geometrical frustration in CBCO is partially lifted.[21] The partially lifted geometrical frustration phenomenon generates a slight disordering of the cobalt spins in the long-range magnetic order. The presence of GP is attributed to a complicated magnetic interaction, competition between AFM and FM orders, while remaining geometrical frustration, which results in inhomogeneity in CBCO.

A series of isothermal magnetization curves around the magnetic transition temperature are assessed to examine the magnetic and magnetocaloric properties of materials. Figure 3(a) shows the M–H curves of the CBCO around T_C under 0 to 7 T. As the temperature rises, the magnetization curves progressively shift from a nonlinear to a linear shape, representing the transition process from FIM to PM. It is worth noting that the M–H curves exhibit a nonlinear behavior at a temperature segment higher than T_C (60–70 K) in the PM region, implying that the PM state is incomplete. Moreover, the sudden change in the slope of some M–H curves suggests the presence of magnetic inhomogenity in this sample.

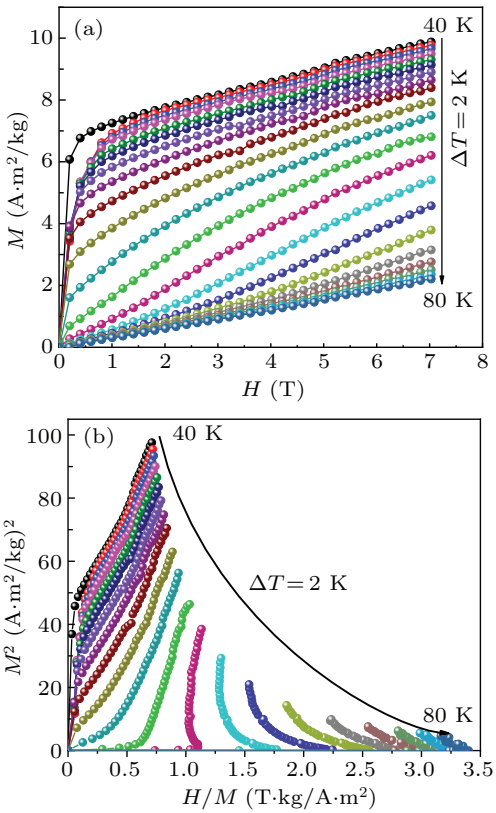


Fig. 3. (a) Series of isothermal M–H curves under magnetic field up to 7 T in the temperature range of 40–80 K. (b) The Arrott plots obtained from the M–H curves.

The Arrott plots identified as H/M versus M^2 were depicted in Fig. 3(b), which is used to explain the nature of the magnetic phase transition in terms of the criterion of Banerjee.[22] For this study, the Arrott plots reveal two distinct regions with separate behaviors relating to the FIM and PM phase. The curves of H/M versus M^2 are approximately linear in the high field region, but they do not constitute a set

of parallel lines, implying that the mean-field theory does not describe magnetic interactions. Meanwhile, a non-linear characteristic with two opposing sides is identified in the low-field region, which can be attributed to different phase orders above and below T_C. At $T < T_C$, the slope of the Arrott plots is positive, implying the second-order characteristic of the magnetic phase transition. For $T > T_C$, the S-shaped magnetization curves with a negative slope are observed, indicating the characteristic of the first-order transition. Therefore, the Arrott plots imply that the magnetic phase transition in CBCO is one of the crossover between the first and second-order magnetic phase transitions.

3.3. Magnetocaloric characterization

To determine the magnetocaloric properties, the isothermal magnetization was measured as a function of the magnetic field in the range 0–7 T and the temperature range of 20 K around the magnetic phase transition temperature. The magnetic entropy change $\Delta S_M(T)$, an essential parameter to represent the magnetocaloric effect of a material, can be indirectly evaluated from the total isothermal magnetization using Maxwell's thermodynamic relation:

$$\left(\frac{\delta S}{\delta H}\right)_T = \left(\frac{\delta M}{\delta T}\right)_H, \tag{3}$$

$$\Delta S_M = \int_{H_1}^{H_2} \left(\frac{\delta M(T,H)}{\delta T}\right)_H \mathrm{d}H. \tag{4}$$

Based on the fact that the isothermal $M(H)$ curve is determined by different changes in the magnetic field and Eq. (4) gives the value of $\Delta S_M(T)$ at different temperatures and fields, $\Delta S_M(T)$ can be expressed as

$$\Delta S_M(T) = \frac{\int_0^H M_i(T,H)\,\mathrm{d}H - \int_0^H M_{i+1}(T,H)\,\mathrm{d}H}{T_i - T_{i+1}}, \tag{5}$$

where M_i and M_{i+1} are the magnetization values measured at T_i and T_{i+1} under a magnetic field of H, respectively. Figure 4(a) shows the magnetic entropy $-\Delta S_M(T)$ calculated using Eq. (5) against temperature for a magnetic field change up to 7 T with steps of 1 T. The maximum peaks occur near T_C, and the values rise as the magnetic field increases. At the field of 7 T, the maximum $-\Delta S_M(T)$ is about 3 J/kg·K at $\sim$ 60 K. It is specially essential to mention that the behaviors of $-\Delta S_M(T)$ below and above T_C differ from each other. A progressive increase in $-\Delta S_M(T)$ occurs below T_C, which is the signature of the second-order phase transition (SOPT); whereas above T_C, the rapid change in $-\Delta S_M(T)$ suggests the first-order phase transition (FOPT) behavior in this region.

The $\Delta S_M(T)$ value of CBCO is comparable with those of some potential magnetic refrigerant material in a similar temperature region under a 5 T magnetic field, such as Gd_2Ni_2Sn (4.6 J/kg·K at 75 K),[23] Tb_2Ni_2Sn (2.9 J/kg·K at 66 K),[23] Sm_2Co_2Ga (1.31 J/kg·K at 62 K),[24] $Nd_6Co_2Si_3$ (5.3 J/kg·K at 84.5 K),[25] TbPtMg (5.1 J/kg·K at 58 K),[26] and GdCuMg (5.6 J/kg·K at 78 K).[27]

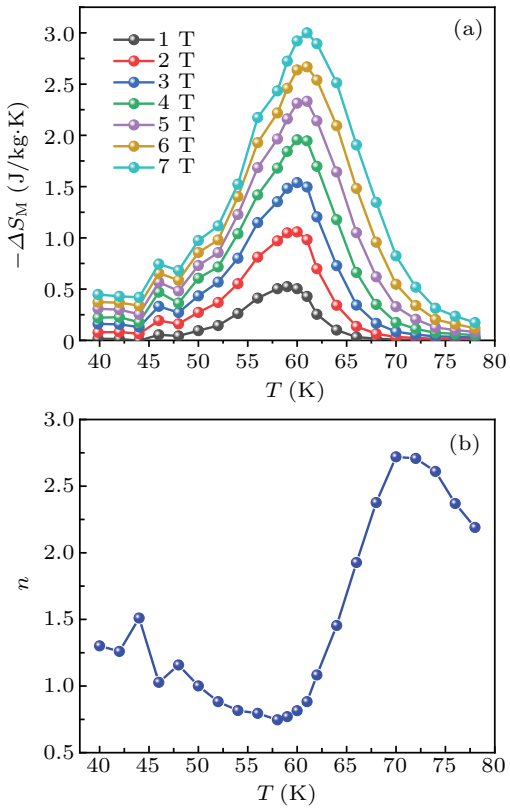


Fig. 4. (a) The $-\Delta S_M(T)$ curves versus temperature under different magnetic fields up to 7 T. (b) The corresponding exponent n as a function of temperature for 7 T.

Dhanasekhar *et al.* reported that the magnetic entropy change of a polycrystalline CBCO sample sintered under various conditions has different values.[16] Compared to the previous report with the decrease in sintering time, a broad peak in magnetic entropy change with the width of half maximum of ΔS–T curve about 14 K is observed in our case. Reduced sintering time contributes to increased porosity. The saturation magnetization decreases with reduced sintering times, which can be attributed to the core/shell morphology, lower grain size and the spin structure on the core and surface. The effect of reducing the sintering time on saturation magnetization is consistent with the previous studies.[28,29]

The Landau theory is a theoretical model which is defined based on the magnetoelastic contribution and electron interaction. This theory is used to determine the nature of the magnetic phase transition in magnetic materials.[30] The Landau theory can verify the nature of the phase transition indicated by other models, as well as explain the magnetic entropy change dependence on temperature variation. The Gibbs free energy for a magnetic system can be described as a function of the magnetic field, magnetization, and temperature in the Landau theory around the Curie temperature transition T_C.

The $G(M,T)$ can be defined in terms of the order parameter of power M, and the coefficients are smooth functions of temperature:[31]

$$G(T,M) = \frac{1}{2}a(T)M^2 + \frac{1}{4}b(T)M^4 + \frac{1}{6}c(T)M^6 + \cdots - \mu_0 HM, \quad (6)$$

where the coefficients $a(T)$, $b(T)$, and $c(T)$ are known as Landau coefficients, and they describe temperature-dependent parameters. The energy $G(M,T)$ corresponds to the minimum value at the phase transition under the condition of equilibrium energy minimization, $(\mathrm{d}G/\mathrm{d}M) = 0$, leading to the following magnetic equation of state:

$$\frac{H}{M} = a(T) + b(T)M^2 + c(T)M^4. \quad (7)$$

The temperature-dependent parameters of $a(T)$, $b(T)$, and $c(T)$ obtained from the polynomial fit of the M–H data using Eq. (7) allow us to determine the order of magnetic phase transition as depicted in Figs. 5(a)–5(c). It is clear from Fig. 5(a) that the parameter $a(T)$ changes from negative to positive as the temperature increases, and the temperature corresponding to zero is almost close to T_C. According to the Inoue–Shimizu model,[32] the sign of the $b(T_C)$ determines the order of the magnetic phase transition, which indicates the FOMT if $b(T_C) < 0$ and the SOPT if $b(T_C) \geq 0$. The sign of $b(T_C)$ is positive in the CBCO sample, confirming the SOPT at T_C. However, as seen above the T_C (near 65 K), the trend of the $b(T)$ is changed. This conclusion matches with the results of the Arrott plots.

The magnetic entropy change is estimated theoretically using the Landau theory through differentiation of the free energy with regard to temperature:

$$-S_M = \left(\frac{\partial G}{\partial T}\right)_H = \frac{1}{2}a'(T)M^2 + \frac{1}{4}b'(T)M^4 + \frac{1}{6}c'(T)M^6. \quad (8)$$

Here, $a'(T)$, $b'(T)$, and $c'(T)$ have been obtained from the temperature derivatives of Landau parameters. Figure 5(d) shows the experimental (red symbols) and calculated (black line) $-\Delta S_M(T)$ versus temperature under 7 T obtained by the Maxwell integration and the Landau theory from $M(T,H)$, respectively. According to recent studies, the magnetoelastic coupling induced a large change in electrical polarization at the PM to FIM phase transition around T_C, as well as explaining the temperature dependence of unit-cell characteristics and volume below T_C.[33,34] The good agreement between the two curves for the CBCO sample implies that the magnetic entropy change versus temperature could be described by magnetoelastic coupling and electron interaction. It can be seen that in the $T > T_C$ region, there is a small discrepancy between the two curves. The difference could be explained by the presence of short-range FM interaction in this area.

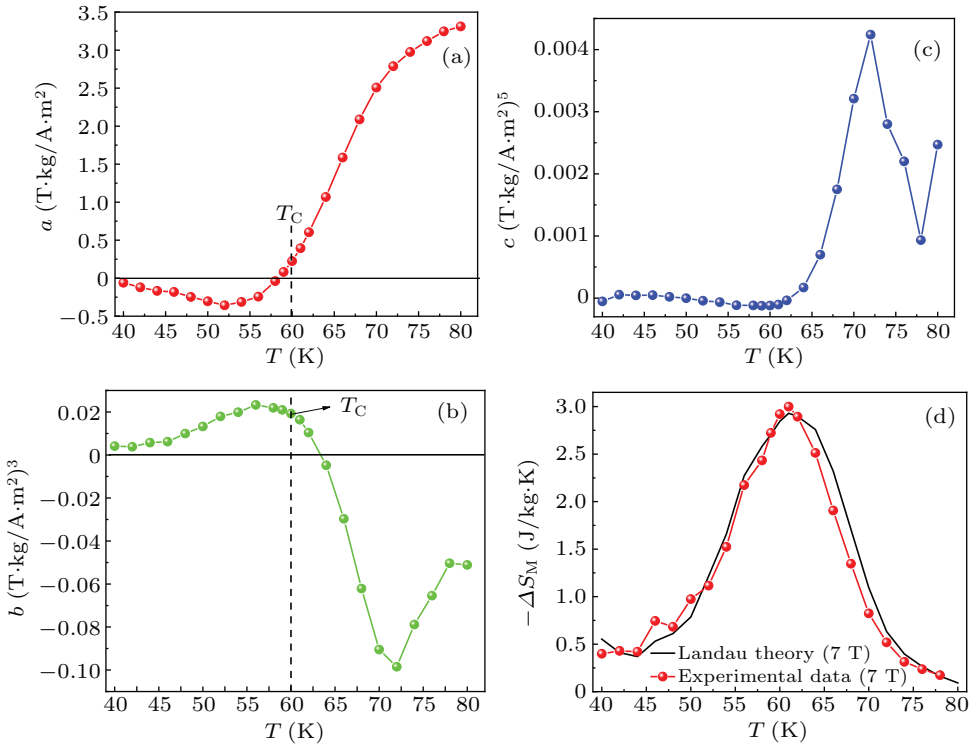


Fig. 5. (a)–(c) The temperature dependence of the Landau parameters. (d) Comparison of experimental and calculated values by the Landau theory of the magnetic entropy change under magnetic field of 7 T for the CBCO sample.

Another method for determining the magnetic phase transition order is to obtained power n from the function $-\Delta S_{\rm M}(T) = a(H^n)$.[35] Figure 4(b) displays the temperature dependence of n versus T in 7 T. The $n(T)$ was calculated for a high field because the multi-domain state exists in a small field. It is impossible to consider the value of n for a small field. According to the CW law, the value of exponent n must be 2 for SOPT in the PM area, whereas in FOPT-type transition it should be $n > 2$. Around the $T_{\rm C}$, the minimum of $n(T)$ is obvious and in the area below the $T_{\rm C}$, the value of $n(T)$ is found to be nearly 1. Above the $T_{\rm C}$ ($T <\sim 65$ K), the curve predicts the second-order phase transition, but there is a significant overshoot in the PM region above 65 K, which indicates the first-order transition. Therefore, it is possible that there is a cross from second-order to first-order transition with increasing temperature.

Franco and co-workers introduced the phenomenological universal master curve as an additional approach to confirm the magnetic phase transition order.[36,37] According to this process, for material undergoing a SOPT, the universal curve assembled by the normalizing magnetic entropy change $(\Delta S_{\rm M}/\Delta S_{\rm M}^{\rm Peak})$ in various applied fields versus rescaling the temperature axis (θ) below and above $T_{\rm C}$ would converge into a single curve. For the CBCO compound, the universal curve is shown in Fig. 6, which is defined as

$$\theta = \begin{cases} \frac{-(T-T_{\rm C})}{(T_{\rm r1}-T_{\rm C})}, & T \le T_{\rm C}, \\ \frac{(T-T_{\rm C})}{(T_{\rm r2}-T_{\rm C})}, & T > T_{\rm C}, \end{cases} \tag{9}$$

where $T_{\rm r1}$ and $T_{\rm r2}$ are temperatures for each curve corresponding to the reference points below and above the $T_{\rm C}$, respectively. $\left(\Delta S_{\rm M}/\Delta S_{\rm M}^{\rm Peak}\right) = f$ is used to evaluate the reference temperature, in which f can be selected from 0 to 1, but too large a value and too small a value would cause large numerical errors. In our case, $f = 0.5$ has been selected for all the curves. As is evident from Fig. 6, the rescaled curves are not completely collapsed into a single curve (especially for $\theta < 0$), confirming the presence of both magnetic transitions.

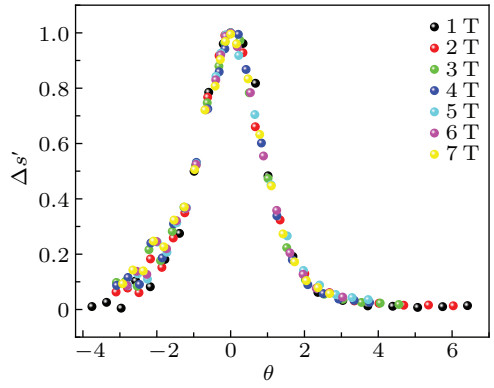


Fig. 6. Universal scaling plot of normalized magnetic entropy change as a function of rescaled temperature.

The large magnetic entropy change is not a sufficient tool to determine the suitability of the material used in magnetic refrigeration. There is a figure of merit to identify the cooling capacity of MCE performance of a magnetic refrigeration material named as refrigeration capacity. The physical concept of refrigeration capacity (RC) is the amount of thermal energy transferred between the hot and cold sources in an ideal cooling cycle.[38] The RC value depends on the height and width of the peak on the magnetic entropy change versus the temperature curve. The common and popular methods to calculate the cooling capacity are given as $\mathrm{RCP} = |\Delta S_{\rm M}^{\rm max}| \cdot \delta T_{\rm FWHM}$ (relative cooling power), where $\delta T_{\rm FWHM}$ is the full width at half maximum of the maximum entropy change, while $\mathrm{RC} = \int_{T_{\rm cold}}^{T_{\rm hot}} |\Delta S_{\rm M}|\, {\rm d}T$. The RCP and RC values of CBCO at 7 T are 42 J/kg and 32.7 J/kg, respectively, as shown in Fig. 7. The large value of RCP obtained for the sample compared to that reported by Dhanasekhar *et al.*[16] because of the border peak can be used to demonstrate the crossover of the first-order to second-order magnetic phase transition, as well as the effect of the preparation condition method. The results give new aspects of the properties of CBCO as potential candidates for such applications.

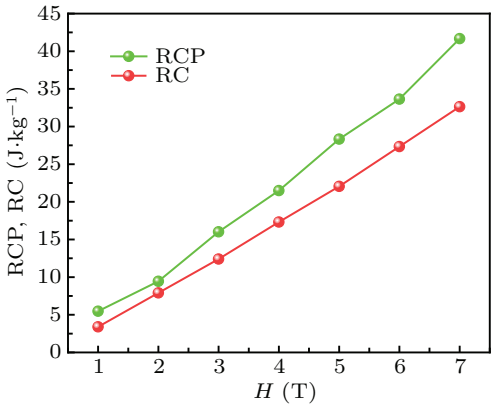


Fig. 7. The relative cooling power curves of the CBCO sample as a function of temperature under different magnetic fields up to 7 T.

4. Conclusion

In summary, we have investigated the magnetic and magnetocaloric features of CBCO, including the type of magnetic transition, the GP-singularity, the universal curve, and power law dependence of magnetic entropy on the magnetic field. The crossover between the first-order and second-order magnetic phase transitions is noticeable in the experimental results and theoretical estimations of the MCE and magnetization of the CBCO compound. The mixed valence of Co, charge ordering, and structural disordering distortion, which generate geometrical frustration, are assumed to govern the physical mechanism. It is worth noting that geometrical frustration has persisted in the PM region, producing inhomogeneity and inducing disordering of the Co spins. The evidence reveals that

short-range magnetic clusters occur in the PM region. The presence of the GP in CBCO is also confirmed. The magnetic entropy changes calculated by the experimental data and the Landau theory have a good match, indicating that magnetoelastic coupling and electron interaction are significant in the magnetocaloric properties of this sample.

Acknowledgements

Project supported by the National Natural Science Foundation of China (Grant No. 51725104) and Beijing Natural Science Foundation (Grant No. Z180009).

References

[1] Omote H, Watanabe S, Matsumoto K, Gilmutdinov I, Kiiamov A and Tayurskii D 2019 *Cryogenics* **101** 58
[2] Zhang H, Gimaev R, Kovalev B, Kamilov K, Zverev V and Tishin A 2019 *Physica B* **558** 65
[3] Pakhira S, Mazumdar C, Ranganathan R, *et al.* 2017 *Sci. Rep.* **7** 7367
[4] Zhang Y 2019 *J. Alloys Compd.* **787** 1173
[5] Taboada-Moreno C A, Sánchez-De Jesús F, Pedro-Garcí a F, Cortés-Escobedo C A, Betancourt-Cantera J A, Ramírez-Cardona M and BolarínMiró A M 2020 *J. Magn. Magn. Mater.* **496** 165887
[6] Franco V, Blázquez J S, Ipus J J, Law J Y, Moreno-Ramírez L M and Conde A 2018 *Prog. Mater. Sci.* **93** 112
[7] Li L, Yan M 2020 *J. Alloys Compd.* **823** 153810
[8] Gottschall T, Skokov K P, Fries M, Taubel A, Radulov I, Scheibel F, Benke D, Riegg S and Gutfleisch O 2019 *Adv. Energy Mater.* **9** 1901322
[9] Bordács S, Kocsis V, Tokunaga Y, Nagel U, Rõ om T, Takahashi Y, Taguchi Y and Tokura Y 2015 *Phys. Rev. B* **92** 214441
[10] Dey K, Indra A, Chatterjee A, Majumdar S, Rütt U, Gutowski O, Zimmermann M V and Giri S 2017 *Phys. Rev. B* **96** 184428
[11] Chai Y S, Cong J Z, He J C, Su D, Ding X X, Singleton J, Zapf V and Sun Y 2021 *Phys. Rev. B* **103** 174433
[12] Qu Z, Ling L, Zhang L, Pi L and Zhang Y 2011 *Solid State Commun.* **151** 917
[13] Seikh M M, Kundu A K, Caignaert V and Raveau B 2016 *J. Alloys Compd.* **656** 166
[14] Hussain S and Maqsood A 2007 *J. Magn. Magn. Mater.* **316** 73
[15] Paul-Boncour V and Bessais L 2021 *Magnetochemistry* **7** 13
[16] Dhanasekhar C, Das A and Venimadhav A 2016 *J. Magn. Magn. Mater.* **418** 76
[17] Caignaert V, Pralong V, Maignan A and Raveau B 2009 *Solid State Commun.* **149** 453
[18] Ghorai S, Ivanov S A, Skini R and Svedlindh P 2021 *J. Phys.: Condens. Matter* **33** 145801
[19] Anderson P W and Hasegawa H 1955 *Phys. Rev.* **100** 675
[20] Fita I, Troyanchuk I O, Zajarniuk T, Iwanowski P, Wisniewski A and Puzniak R 2018 *Phys. Rev. B* **98** 214445
[21] Caignaert V, Pralong V, Hardy V, Ritter C and Raveau B 2010 *Phys. Rev. B* **81** 094417
[22] Banerjee B 1964 *Phys. Lett.* **12** 16
[23] Kumar P, Singh N K, Suresh K G and Nigam A K 2008 *Phys. Rev. B* **77** 184411
[24] Morozkin A V, Garshev A V, Yapaskurt V O, Yao J, Nirmala R, Quezado S and Malik S K 2018 *J. Solid State Chem.* **260** 95
[25] Shen J, Li Y X and Sun J R 2009 *J. Alloys Compd* . **476** 693
[26] Zhang Z, Stein S, Li L and Poettgen R 2019 *Intermetallics* **109** 24
[27] Stein S, Heletta L, Block T and Pöttgen R 2018 *Z. Naturforsch. B* **73** 987
[28] Aliuzzaman M, Haque M M, Ferdous M J, Hoque S M and Hakim M A 2014 *World J. Condens. Matter Phys.* **4** 13
[29] Ajmal M, Shah N A, Maqsood A, Awan M S and Arif M 2010 *J. Alloys Compd.* **508** 226
[30] Amaral J S, Reis M S, Amaral V S, Mendonca T M, Araujo J P, Sa M A, Tavares P B and Vieira J M 2005 *J. Magn. Magn. Mater.* **290** 686
[31] Nasri M, Cherif A and Dhahri E 2019 *J. Low Temp. Phys.* **196** 386
[32] Inoue J and Shimizu M 1982 *J. Phys. F: Met. Phys.* **12** 1811
[33] Johnson R D, Cao K, Giustino F and Radaelli P G 2014 *Phys. Rev. B* **90** 045129
[34] Singh K, Caignaert V, Chapon L C, Pralong V, Raveau B and Maignan A 2012 *Phys. Rev. B* **86** 024410
[35] Law J Y, Franco V, Moreno-Ramírez L M, Conde A, Karpenkov D Y, Radulov I, Skokov K P and Gutfleisch O 2018 *Nat. Commun.* **9** 1
[36] Bonilla C M, Bartolomé F, García L M, Parra-Borderías M, HerreroAlbillos J and Franco V 2010 *J. Appl. Phys.* **107** 09E131
[37] Franco V, Blázquez J S and Conde A 2006 *Appl. Phys. Lett.* **89** 222512
[38] Yang Y, Zhang Y, Xu X, Geng S, Hou L, Li X, Ren Z and Wilde G 2017 *J. Alloys Compd.* **692** 665